Co-published by
Institute of Fluid-Flow Machinery
Polish Academy of Sciences
Committee on Thermodynamics and Combustion
Polish Academy of Sciences

http://www.imp.gda.pl/archives-of-thermodynamics/

Influence of spacing of waterwall tubes on their operating parameters

Marek Majdak

Cracow University of Technology, Faculty of Environmental Engineering and Energy, Department of Energy, Warszawska 24, 31-155 Cracow, Poland
Author email: marek.majdak@pk.edu.pl

Received: 01.10.2025; revised: 20.03.2026; accepted: 22.04.2026

Abstract

The article presents the results of thermal and flow analysis of the working conditions of neighbouring waterwall tubes, loaded with heat streams of different values for two different widths of tube spacing. The numerical model used for the analysis allows us to calculate the temperature distribution at the tubes and in the fluid flowing through them at each time step, depending on the thermo-physical parameters of the fluid and the material from which the tubes and fins were made. By using the algorithm, it is possible to precisely determine the three-dimensional temperature distribution for tubes, allowing us to determine the places where the most divergent temperatures occur and in which thermal stresses of the highest value may occur. The analysis of several adjacent tubes will allow for determining the effect of temperature differences in the tubes and fins connecting them, and to collect data that may be used for the determination of stress distribution in the tubes and fins. In the presented case 3, smooth tubes connected by fins were used, and the heat flux on the centre tube was by 50% higher than on the outer ones.

Keywords: Waterwall tube; Supercritical steam boiler; Temperature distribution; Thermal stresses

Vol. 47(2026), No. 2, 87–97; doi: 10.24425/ather.2026.158676

Cite this manuscript as: Majdak, M. (2026). Influence of spacing of waterwall tubes on their operating parameters. *Archives of Thermodynamics*, 47(2), 87−97.

1. Introduction

In subcritical boilers, the heat flux distribution on the width of the combustion chamber wall is close to uniform. Therefore, the temperature of the walls of neighbouring waterwall tubes is similar. In supercritical boilers, the heat flux distribution on the width of the combustion chamber wall is uneven – on the centre of the wall, its value is about 50% higher than close to the combustion chamber corners [1].

The most common method of reduction of thermal stresses resulting from uneven heating of neighbouring waterwall tubes is differentiation of mass flux of fluid flowing inside tubes – the mass flow in tubes near the centre of the combustion chamber wall is higher than in tubes close to the corners of the combustion chamber. Another method analysed by designers of combustion chambers is to vary the spacing of the waterwall tubes. In some publications, the idea of reducing the spacing near the centre of the combustion chamber wall to increase the number of waterwall tubes on the unit width of the wall is presented.

2. Literature review

Many publications may be found in the literature regarding the heat and mass transfer in subcritical and supercritical boilers. Authors of [2] proposed one of the first computer-based monitoring systems for boilers with natural water circulation. A computer system allows the calculation of, among others, the boiler efficiency, combustion gas mass flow rate, and heat load at the walls of the combustion chamber. The results of the calculations were validated with the measurement data.

Nomenclature

A – tube cross-section surface area, m^2
c – specific heat per mass unit, kJ/(kg·K)
$d\tau$ – time step, s
e – energy per fluid mass, J/kg
g – gravitational acceleration, m/s^2
i – enthalpy, kJ/kg
$\dot{m}$ – mass flow
p – pressure, kPa
q – heat flux, W/m^2
r – radius, m
s – tube spacing, m
t – fluid temperature, °C
u – unit internal energy, J/kg
U – tube perimeter, m
V – fluid volume, m^3

Greek symbols

α – heat transfer coefficient, W/(m^2·K)
Δr – tube wall thickness, m
ΔV – finite volume, m^3
Δx – fin width, m
Δz – length of control volume, m
$\Delta \varphi$ – characteristic angle, -
δ –thickness, m
θ – temperature of wall material, °C
λ – thermal conductivity, W/(m·K)
ρ – density, kg/m^3
σ_τ – tangential stresses, N/m^2
τ – time, s

Subscripts and Superscripts

in – inner
j – spatial step number
m – medium
o – outer
tw – tube wall
τ – time step number
w – wall

Experimental measurements performed for the ultra-supercritical boiler were presented in [3]. Authors of the publication monitored the main thermal and flow parameters of steam flowing inside the waterwall tube for different steam pressures and boiler loads. During the tests, steam reached subcritical, near-critical and supercritical pressures, so the conclusions drawn from the analysis of the results can be successfully applied to a wide range of steam flows.

Results of numerical simulations of thermo-physical parameters of supercritical steam were also presented in [4]. A four-pass steam superheater was used as an analysis system for the calculation of the specific heat of steam based on the temperature and pressure of steam, and the temperature of the waterwall tube wall. The heat transfer of a cross-counter-current superheater consisting of 48 tubes was analysed.

Spirally rifled waterwall tubes are used in power boilers to reduce thermal stresses and allow faster heat-transfer stabilisation. Results of numerical simulations of thermal and flow phenomena for smooth and internally ribbed tubes mounted vertically were presented by the authors of [5−8]. The calculations were performed to examine the temperature and thermal stress distributions in tubes, and the thermo-physical parameters of the working fluid. In [7], numerical data were also verified with experimental data from the measurement performed on the dedicated experimental stand.

Authors of [9] presented the results of experimental studies on the application of internally rifled vertical tubes in a combustion chamber. They have listed the advantages of this system of waterwall tubes compared to spirally wound smooth tubes. In the paper, the main advantages of using internal spirally rifled tubes can be found in the field of installation, flow characteristics, flow stability and load follow-up capability, as well as a short analysis of possible directions for optimising this type of system was presented.

Another possibility of minimising the thermal and pressure stresses can be the use of corrugated furnace tubes. Authors of [10] analysed stress distribution for different corrugations of depths and spacings of the tube. It was found that in this high-power fire-tube boiler, a corrugated furnace tube with a greater corrugation depth should be used, because it allows for the reduction of the maximum value of stresses in the structure.

In publications [11−13], cases were analysed considering the influence of the variability of heat load with increasing height above the inlet to the waterwall tubes on the thermo-physical parameters of walls and tubes. In the analysed studies, an additional measuring insert was used, located on the front wall of the tube, which allowed for obtaining more accurate temperature values.

Waterwall tubes mounted on the combustion chamber walls are heated on one side, which results in a significant temperature difference between front and rear tube walls [14,15]. Due to the uneven temperature distribution in the cross-sections of the tubes, their division into smaller elements is often analysed. In publications [16−20], a model of the division of the half cross-section of the waterwall tube with the fin on the control volumes was presented. In the articles, temperature distributions in tubes and fins were presented, obtained by simulation performed for the operating parameters of a supercritical boiler.

Authors of [21] analysed the temperature distribution in the wall of the waterwall tube covered with ash deposits on the outer surface of the tube. The calculation of heat transfer for tubes with scale deposits on the inner surface of the tube was also presented. A complex numerical model can be used for calculations for steam, tube wall, and flue gas temperature for the entire superheater.

In the article [22], the results of numerical simulation carried out by using the Runge-Kutta method to solve the equations of energy, mass and momentum balance were presented. The authors proposed a calculation algorithm for the medium flowing inside the waterwall tubes of the furnace chamber. The presented results were based on parameters of the supercritical furnace with a steam capacity of 2400×10^3 kg/h.

The computational models proposed in the literature allow for carrying out calculations for one or several waterwall tubes, with various calculation details. The novelty proposed in this publication will be the analysis of the change in temperature distribution depending on the width of spacing of the waterwall tubes under the same initial conditions.

3. Problem analysis

In the article, an analysis of temperature distribution in waterwall tubes connected by fins was presented. The proposed model allows for determining the three-dimensional temperature distribution, which will be presented for the cross-sections of waterwall tubes and fins between them, taking into account the variability of thermo-physical parameters of fluids and tubes in every control volume at each time step.

The analysis was performed by using parameters of water and steam calculated on the basis of the International Association for the Properties of Water and Steam table and the properties of 13CrMo4-5 steel received from its manufacturer.

As input data, the operating parameters from the supercritical boiler operating in one of the Polish power plants were used. Due to the fact that the boiler generates steam with supercritical parameters, the analysis took into account the uneven distribution of the heat flux density across the width of the combustion chamber wall. Based on experimental studies conducted by many teams, it was determined that the heat flux incident on the combustion chamber walls near the corners is up to 50% lower than the heat flux incident on the wall at half its width at the same height; a graphical interpretation of this condition is presented in Fig. 1 [1].

The model of the division of the cross-section of waterwall tubes connected by fins was proposed in [23,24]. In the cross-section of the tube with two halves of fins, 36 characteristic points are identified (Fig. 2); this method of division can be scaled to a system consisting of multiple tubes, as presented for three tubes in Fig. 3.

The energy balance equations written for all elements of the analysed system allow for the determination of the temperature distribution in the waterwall tubes connected by fins. Equations for selected control volumes are presented below.

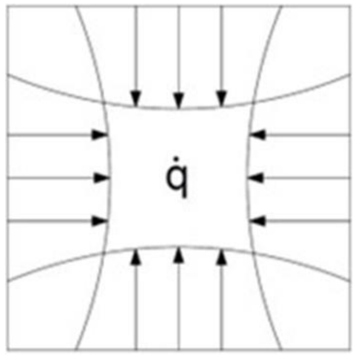

Fig. 1. The distribution of the thermal flux density in the cross-section of the supercritical boiler's furnace chamber.

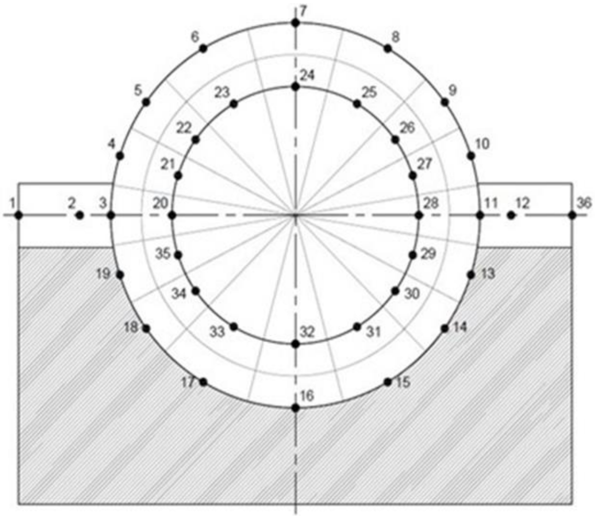

Fig. 2. The method of division of the cross-section of the waterwall tube with two halves of fins into control volumes.

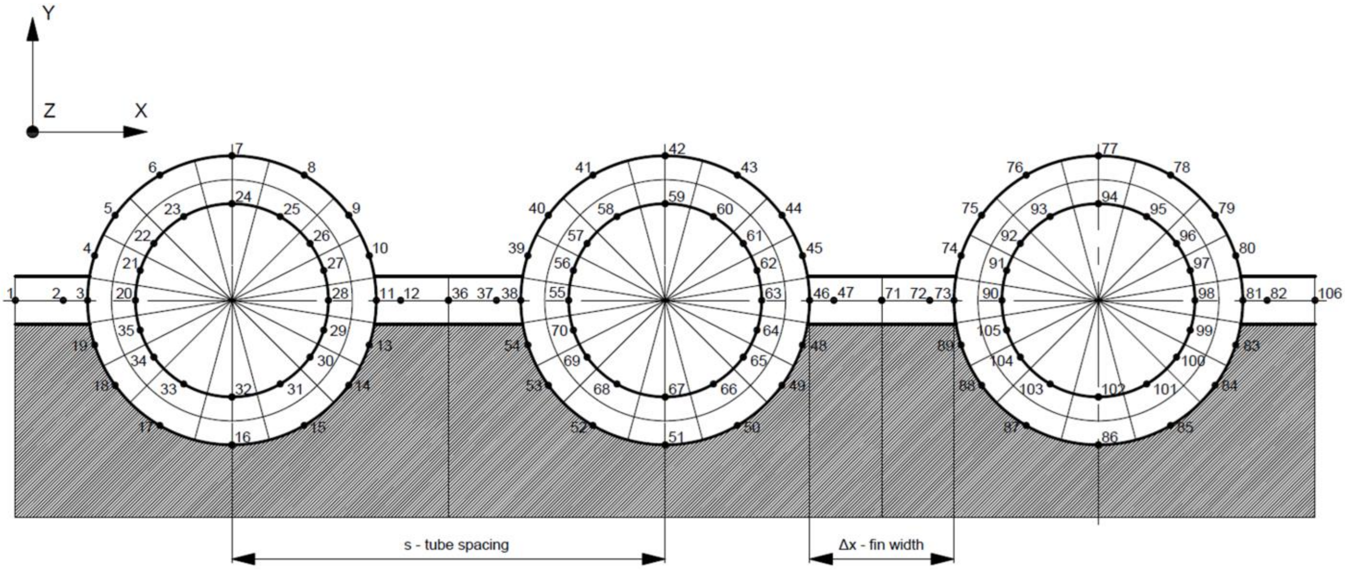

Fig. 3. The division of the cross-section of three waterwall tubes with fins into control volumes with the adopted coordinate system.

For the point on the centre of the outer surface of the front wall of the tube (“7” in Fig. 4), the energy balance equation takes the form of Eq. (1). Analogical equations can be obtained for points “42” and “77” by increasing the numbers in the lower index by 35 or 70, respectively.

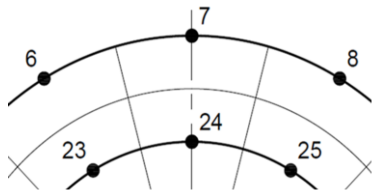

Fig. 4. The control areas containing points 7 and 24.

$$c_{7,j}\rho_{7,j}\frac{\Delta\hat{\varphi}_1}{2}(r_o^2-r_m^2)\Delta z\frac{d\theta_{7,j}}{d\tau}=\lambda_{7,j}\frac{\theta_{6,j}-\theta_{7,j}}{\Delta\hat{\varphi}_1 r_o}\frac{\Delta r}{2}\Delta z+$$
$$+\lambda_{7,j}\frac{\theta_{8,j}-\theta_{7,j}}{\Delta\hat{\varphi}_1 r_o}\frac{\Delta r}{2}\Delta z+\lambda_{7,j}\frac{\theta_{24,j}-\theta_{7,j}}{\Delta r}\Delta\hat{\varphi}_1 r_m\Delta z+$$
$$+\lambda_{7,j}\frac{\Delta\hat{\varphi}_1}{2}(r_o^2-r_m^2)\frac{\theta_{7,j-1}-\theta_{7,j}}{\Delta z}+$$
$$+\lambda_{7,j}\frac{\Delta\hat{\varphi}_1}{2}(r_o^2-r_m^2)\frac{\theta_{7,j+1}-\theta_{7,j}}{\Delta z}+\dot{q}_{7,j}\Delta\hat{\varphi}_1 r_o\Delta z. \tag{1}$$

For the point on the centre of the inner surface of the front wall of the tube (“24” in Fig. 4), the energy balance equation takes the form of Eq. (2). Analogical equations can be obtained for points “59” and “94” by increasing the numbers in the lower index by 35 or 70, respectively.

$$c_{24,j}\rho_{24,j}\frac{\Delta\hat{\varphi}_1}{2}(r_m^2-r_{in}^2)\Delta z\frac{d\theta_{24,j}}{d\tau}=\lambda_{24,j}\frac{\theta_{25,j}-\theta_{24,j}}{\Delta\hat{\varphi}_1 r_{in}}\frac{\Delta r}{2}\Delta z+$$
$$+\lambda_{24,j}\frac{\theta_{23,j}-\theta_{24,j}}{\Delta\hat{\varphi}_1 r_{in}}\frac{\Delta r}{2}\Delta z+\lambda_{24,j}\frac{\theta_{7,j}-\theta_{24,j}}{\Delta r}\Delta\hat{\varphi}_1 r_m\Delta z+$$
$$+\lambda_{24,j}\frac{\Delta\hat{\varphi}_1}{2}(r_m^2-r_{in}^2)\frac{\theta_{24,j-1}-\theta_{24,j}}{\Delta z}+$$
$$+\lambda_{24,j}\frac{\Delta\hat{\varphi}_1}{2}(r_m^2-r_{in}^2)\frac{\theta_{24,j+1}-\theta_{24,j}}{\Delta z}+$$
$$+\alpha_j\left(t_j-\theta_{24,j}\right)\Delta\hat{\varphi}_1 r_{in}\Delta z. \tag{2}$$

For the point in the centre of the fin between waterwall tubes (“36” in Fig. 5), the energy balance equation takes the form of Eq. (3). An analogical equation can be obtained for point “71” by increasing the number in the lower index by 35. Equations for points “1” and “106” located at the ends of the analysed fragment of the cross-section of the combustion chamber wall can be determined assuming the symmetry of parameters for adjacent characteristic points.

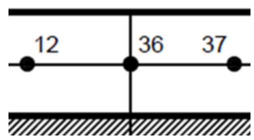

Fig. 5. The control area containing point 36.

$$c_{36,j}\rho_{36,j}\Delta x\delta_w\Delta z\frac{d\theta_{36,j}}{d\tau}=\lambda_{36,j}\frac{\theta_{37,j}-\theta_{36,j}}{\Delta x}\delta_w\Delta z+$$
$$+\lambda_{36,j}\frac{\theta_{12,j}-\theta_{36,j}}{\Delta x}\delta_w\Delta z+\lambda_{36,j}\Delta x\delta_w\frac{\theta_{36,j-1}-\theta_{36,j}}{\Delta z}$$
$$+\lambda_{36,j}\Delta x\delta_w\frac{\theta_{36,j+1}-\theta_{36,j}}{\Delta z}+\dot{q}_{36,j}\frac{\Delta x}{3}\Delta z. \tag{3}$$

After transforming Eqs. (1)–(3), the dependencies for determining the temperature values are obtained in the form of Eqs. (4)–(6):

$$\theta_{7,j}^{\tau+\Delta\tau}=\theta_{7,j}^{\tau}+\frac{\Delta\tau}{c_{7,j}^{\tau}\rho_{7,j}^{\tau}\frac{\Delta\hat{\varphi}_1}{2}(r_o^2-r_m^2)\Delta z}\left[\lambda_{7,j}^{\tau}\frac{\theta_{6,j}^{\tau}-\theta_{7,j}^{\tau}}{\Delta\hat{\varphi}_1 r_o}\frac{\Delta r}{2}\Delta z+\lambda_{7,j}^{\tau}\frac{\theta_{8,j}^{\tau}-\theta_{7,j}^{\tau}}{\Delta\hat{\varphi}_1 r_o}\frac{\Delta r}{2}\Delta z+\lambda_{7,j}^{\tau}\frac{\theta_{24,j}^{\tau}-\theta_{7,j}^{\tau}}{\Delta r}\Delta\hat{\varphi}_1 r_m\Delta z+\right.$$
$$\left.+\lambda_{7,j}^{\tau}\frac{\Delta\hat{\varphi}_1}{2}(r_o^2-r_m^2)\frac{\theta_{7,j-1}^{\tau}-\theta_{7,j}^{\tau}}{\Delta z}+\lambda_{7,j}^{\tau}\frac{\Delta\hat{\varphi}_1}{2}(r_o^2-r_m^2)\frac{\theta_{7,j+1}^{\tau}-\theta_{7,j}^{\tau}}{\Delta z}+\dot{q}_{7,j}^{\tau}\Delta\hat{\varphi}_1 r_o\Delta z\right], \tag{4}$$

$$\theta_{24,j}^{\tau+\Delta\tau}=\theta_{24,j}^{\tau}+\frac{\Delta\tau}{c_{24,j}^{\tau}\rho_{24,j}^{\tau}\frac{\Delta\hat{\varphi}_1}{2}(r_m^2-r_{in}^2)\Delta z}\left[\lambda_{24,j}^{\tau}\frac{\theta_{23,j}^{\tau}-\theta_{24,j}^{\tau}}{\Delta\hat{\varphi}_1 r_{in}}\frac{\Delta r}{2}\Delta z+\lambda_{24,j}^{\tau}\frac{\theta_{25,j}^{\tau}-\theta_{24,j}^{\tau}}{\Delta\hat{\varphi}_1 r_{in}}\frac{\Delta r}{2}\Delta z+\lambda_{24,j}^{\tau}\frac{\theta_{7,j}^{\tau}-\theta_{24,j}^{\tau}}{\Delta r}\Delta\hat{\varphi}_1 r_m\Delta z+\right.$$
$$\left.+\lambda_{24.j}^{\tau}\frac{\Delta\hat{\varphi}_1}{2}(r_m^2-r_{in}^2)\frac{\theta_{24,j-1}^{\tau}-\theta_{24,j}^{\tau}}{\Delta z}+\lambda_{24.j}^{\tau}\frac{\Delta\hat{\varphi}_1}{2}(r_m^2-r_{in}^2)\frac{\theta_{24,j+1}^{\tau}-\theta_{24,j}^{\tau}}{\Delta z}+\alpha_j^{\tau}(t_j^{\tau}-\theta_{24,j}^{\tau})\Delta\hat{\varphi}_1 r_{in}\Delta z\right], \tag{5}$$

$$\theta_{36,j}^{\tau+\Delta\tau}=\theta_{36,j}^{\tau}+\frac{\Delta\tau}{c_{36,j}^{\tau}\rho_{36,j}^{\tau}\Delta x\delta_w\Delta z}\left[\lambda_{36,j}^{\tau}\frac{\theta_{12,j}^{\tau}-\theta_{36,j}^{\tau}}{\Delta x}\delta_w\Delta z+\lambda_{36,j}^{\tau}\frac{\theta_{37,j}^{\tau}-\theta_{36,j}^{\tau}}{\Delta x}\delta_w\Delta z+\right.$$
$$\left.+\lambda_{36,j}^{\tau}\Delta x\delta_w\frac{\theta_{36,j-1}^{\tau}-\theta_{36,j}^{\tau}}{\Delta z}+\lambda_{36,j}^{\tau}\Delta x\delta_w\frac{\theta_{36,j+1}^{\tau}-\theta_{36,j}^{\tau}}{\Delta z}+\dot{q}_{36,j}^{\tau}\frac{\Delta x}{3}\Delta z\right]. \tag{6}$$

In order to determine the average temperature of the fluid in the cross-sections of waterwall tubes, the mass, energy and momentum balance equations were used. The balance equations were used in the form of separable differential equations – on the left side, expressions containing time derivatives were presented, while on the right side, spatial derivatives were replaced using the backward difference quotient method [22].

The mass balance equation takes the form:

$$\frac{\partial(\Delta V\rho)}{\partial\tau}=(A\rho v)|_{z-\left(\frac{\partial z}{2}\right)}-(A\rho v)|_{z+\left(\frac{\partial z}{2}\right)}. \tag{7}$$

The momentum conservation law takes the form:

$$\frac{\partial(Av\rho\Delta z)}{\partial\tau}=(\dot{m}v)|_{z-\left(\frac{\partial z}{2}\right)}-(\dot{m}v)|_{z+\left(\frac{\partial z}{2}\right)}+$$
$$A\cdot\left(p|_{z-\left(\frac{\partial z}{2}\right)}-p|_{z+\left(\frac{\partial z}{2}\right)}\right)-\sigma\tau U\Delta z-\rho g\Delta V\sin\varphi. \tag{8}$$

The energy of the fluid, related to unit mass, must be analysed as a sum of internal, kinetic and potential energy:

$$e=\frac{v^2}{2}+gz\sin\varphi+u. \tag{9}$$

For the purpose of this analysis, it was assumed that the work done by surface and volume forces is negligible. After rearrangements presented in [22], Eq. (9) can be presented in the form of a differential equation with separable variables:

$$\frac{\partial i}{\partial \tau} = \left(1-\frac{1}{\rho}\frac{\partial p}{\partial i}\right)^{-1}\left(\frac{\dot{m}}{A\rho}\left(\frac{1}{\rho}\frac{\partial p}{\partial z}-\frac{\partial i}{\partial z}+\frac{1}{\rho}\frac{\partial p_\tau}{\partial z}\right)+\frac{4\alpha(\theta-t)}{2r_{in}\rho}-\frac{1}{A\rho}\frac{\partial p}{\partial \rho}\frac{\partial \dot{m}}{\partial z}\right). \qquad (10)$$

By using the method presented in [24], balance equations for fluid can be solved and written in a form presented below for each time step "τ" and each spatial step "j", with space derivatives on the left side of the equation and time derivatives replaced with difference quotients on the right side. Therefore, the following equations were applied to the numerical model:

- the energy balance equation:

$$\frac{di_j^\tau}{dz} = \frac{A\rho_j^{\tau-\Delta\tau}}{\dot{m}_j^{\tau-\Delta\tau}}\left(-\frac{i_j^\tau - i_j^{\tau-\Delta\tau}}{\Delta\tau}+4\alpha_j^{\tau-\Delta\tau}\cdot\frac{\theta_j^{\tau-\Delta\tau}-t_j^{\tau-\Delta\tau}}{2r_{in}\rho_j^{\tau-\Delta\tau}}\right), \qquad (11)$$

where the density of the fluid can be found as a function of enthalpy and pressure of the fluid:

$$\rho_j^\tau = f\left(i_j^\tau, p_j^{\tau-\Delta\tau}\right), \qquad (12)$$

- the mass balance equation:

$$\frac{d\dot{m}_j^\tau}{dz} = -A\frac{\rho_j^\tau-\rho_j^{\tau-\Delta\tau}}{\Delta\tau}, \qquad (13)$$

- the momentum balance equation:

$$\frac{d}{dz}\left(\frac{(\dot{m}^2)_j^\tau}{A^2\rho_j^\tau}+p_j^\tau\right) = -\frac{1}{A}\frac{(\dot{m}^2)_j^\tau-(\dot{m}^2)_j^{\tau-\Delta\tau}}{\Delta\tau}-\frac{dp_\tau}{dz}-\rho_j^\tau g\sin\varphi. \qquad (14)$$

Using the relations (11)–(14), the parameters of the fluid in each cross-section of the tube can be determined in each time step. In the proposed model, the heat transfer coefficient for the supercritical fluid flow is calculated on the inner surface of the tube by using the dependency determined by Kitoh et al. [25].

In order to compare the temperature distributions in the waterwall tubes connected by fins of different widths, the operating conditions of a supercritical boiler working in the supercritical stage were used. The geometrical parameters of tubes and fins in the first case were adopted directly from the combustion chamber walls geometry; in the second case, the width of fins between tubes was increased. The working fluid is single-phase because its thermodynamic parameters exceed the water critical point parameters. A model was developed that allows online calculation of parameters of waterwall tubes and working fluid, in which the assumptions mentioned below were taken into account.

The fluid temperature inside the tubes was assumed to be constant; it is also assumed that the parameters of the fluid in the entire cross-section of the tube are the same. Equations for points "1" and "106" located at the ends of the analysed fragment of the cross-section of the combustion chamber wall (Fig. 3) can be determined assuming the symmetry of parameters for adjacent characteristic points. For the purpose of this analysis, it was assumed that the work done by surface and volume forces is negligible. To approximate the actual simulation conditions, a plane strain state was assumed, meaning that there was no deformation in the Z-axis direction perpendicular to the analysed cross-section. One side of the model was fixed to a point, and the other side was blocked from moving relative to the Y-axis.

The most important adopted parameters are:

- mass flow per tube: $\dot{m}$ = 0.77 kg/s,
- water pressure at the tube inlet: p_{in} = 299.6 bar,
- waterwall tube material: 16Mo3 steel,
- outer tube diameter: d_o = 33.7 mm,
- tube wall thickness: δ_{tw} = 6.1 mm,
- tube spacing: s_1 = 50 mm (case 1), s_2 = 58.15 mm (case 2).

For the purpose of the analysis, it was assumed that the average heat flux would vary with the height of the combustion chamber according to the characteristics shown in Fig. 6.

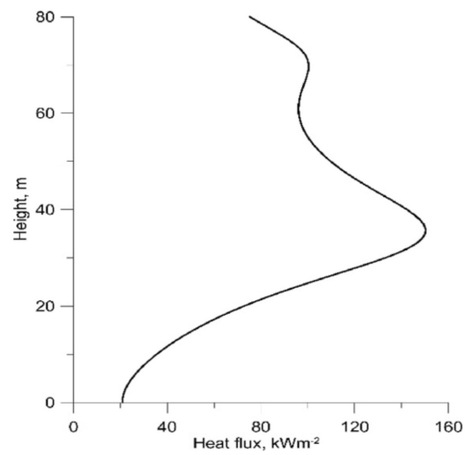

Fig. 6. Distribution of the average heat flux at the furnace waterwalls along the height of the combustion chamber.

The analysed waterwall tubes are 166.5 m long, and the assumed step along the tube length (along the Z axis) is 0.75 m. The entire analysed model was divided into 222 levels with a total number of characteristic points equal to 23 532.

The comparison of temperature values obtained in both cases is presented in the next chapter.

4. Results and discussion

Two cases of heating of the system were analysed, consisting of three tubes connected by fins. In each case, the heat flux on the centre tube was by 50% higher than that on the outer tubes. In the second case, the tube spacing was increased from 50 mm to 58.15 mm to compare the temperature and thermal stress distribution in cross-sections of the analysed tubes.

The temperature distribution at the characteristic points obtained from the developed numerical algorithm was imported into the ANSYS environment as input data and graphically interpolated. Thermodynamic parameters of the material were determined according to data provided by the steel manufacturer.

The mounting conditions for the analysed tube cross-sections and connecting fins were determined, allowing for the simulation of the operating conditions of the entire combustion chamber wall section. On the basis of the imported temperature distribution and determined parameters, the static distribution of the thermal stresses is calculated. Due to the relatively simple geometry analysed in this single case, a 0.25 mm quadrangular mesh was applied to the system.

The temperature distributions obtained using the numerical model for the case with “standard” tube spacing (fin width is equal to 16.3 mm) are presented in Figs. 7–9, for the case with wider tube spacing (fin width is equal to 24.45 mm) in Figs. 10–12. The thermal stress distributions for the case with “standard” tube spacing are presented in Figs. 13–15, for the case with a wider tube spacing in Figs. 16–18.

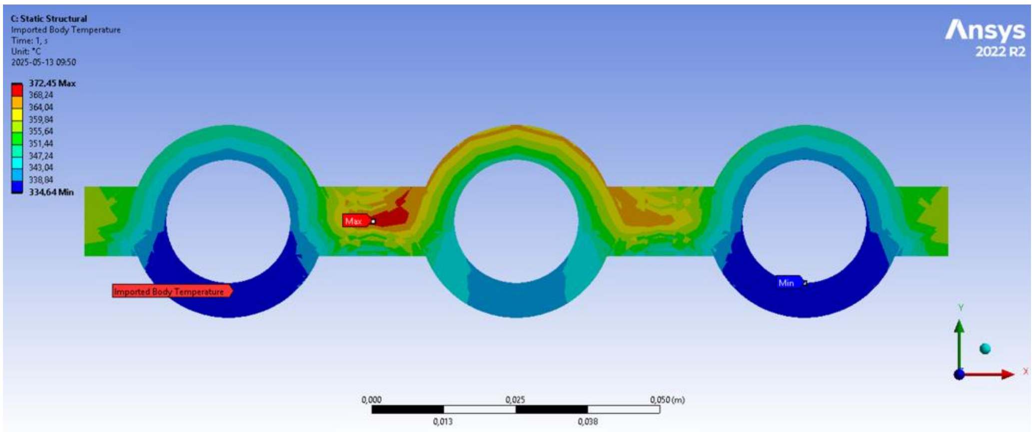

Fig. 7. The temperature distribution in the cross-section of the analysed system with "standard" tube spacing at a distance of 40 m from the tube inlet.

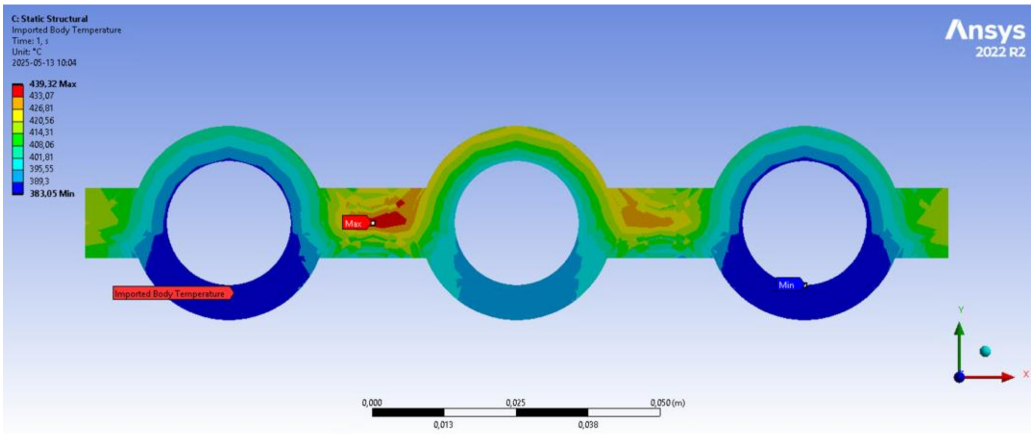

Fig. 8. The temperature distribution in the cross-section of the analysed system with "standard" tube spacing at a distance of 80 m from the tube inlet.

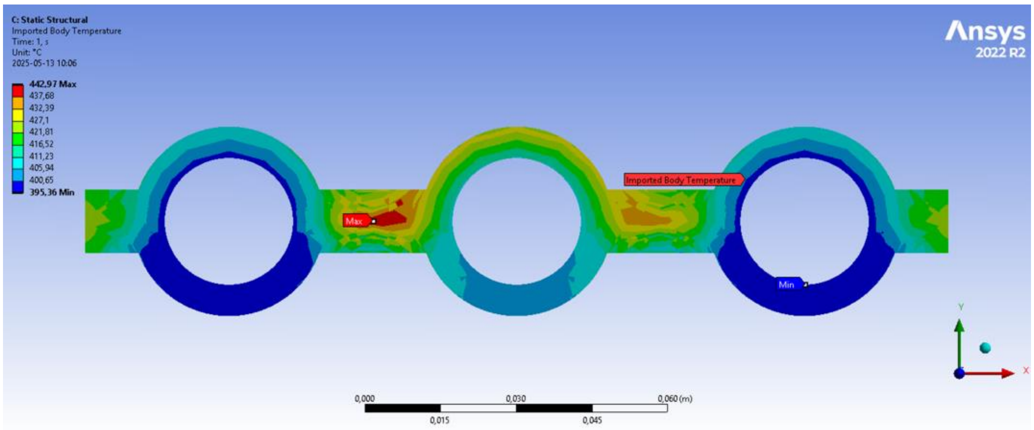

Fig. 9. The temperature distribution in the cross-section of the analysed system with "standard" tube spacing at a distance of 120 m from the tube inlet.

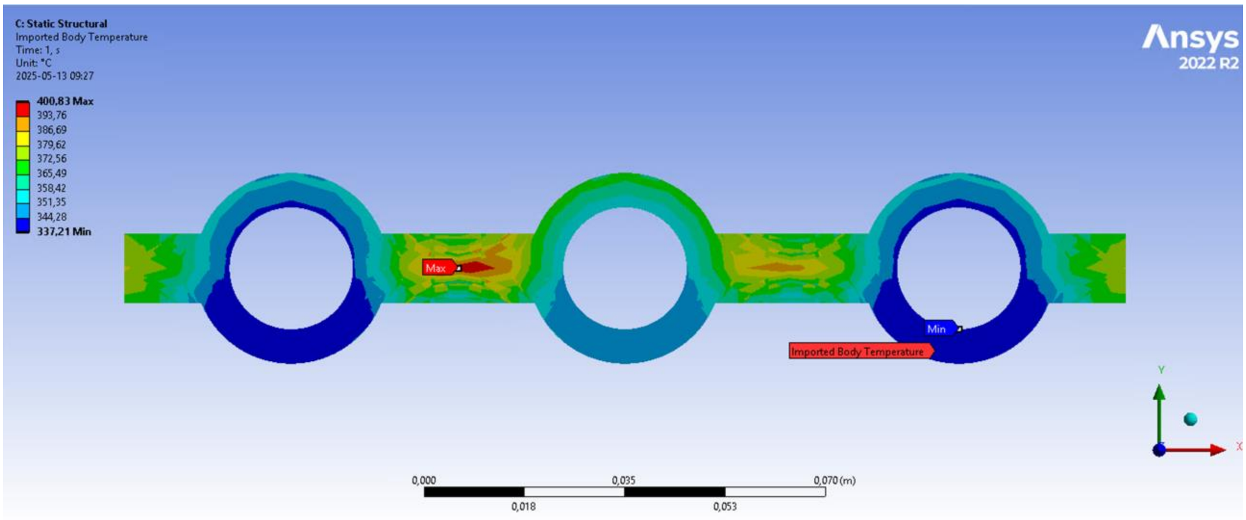

Fig. 10. The temperature distribution in the cross-section of the analysed system with a wider tube spacing at a distance of 40 m from the tube inlet.

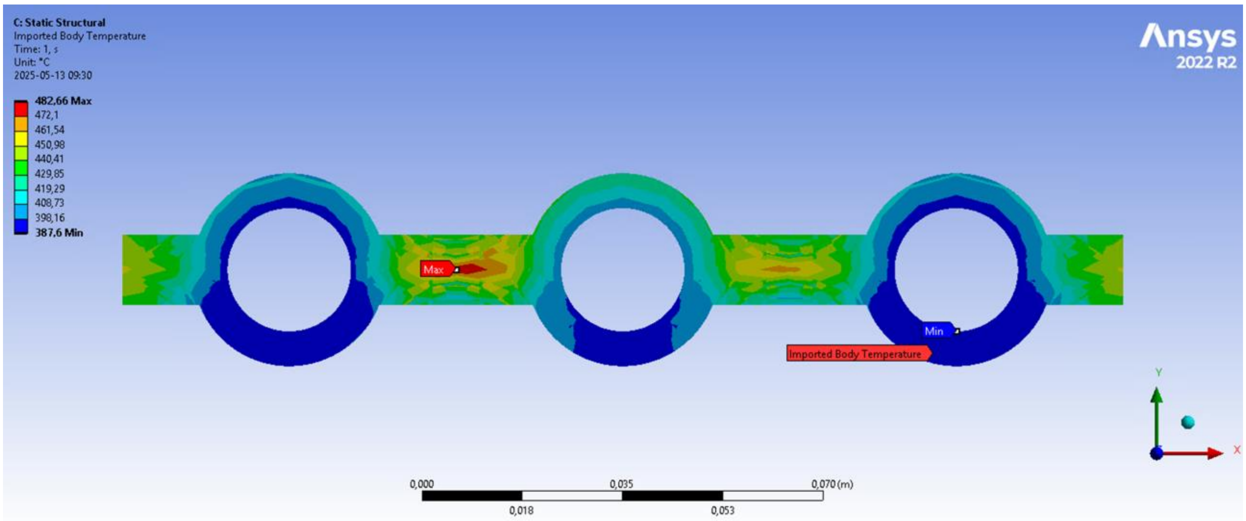

Fig. 11. The temperature distribution in the cross-section of the analysed system with a wider tube spacing at a distance of 80 m from the tube inlet.

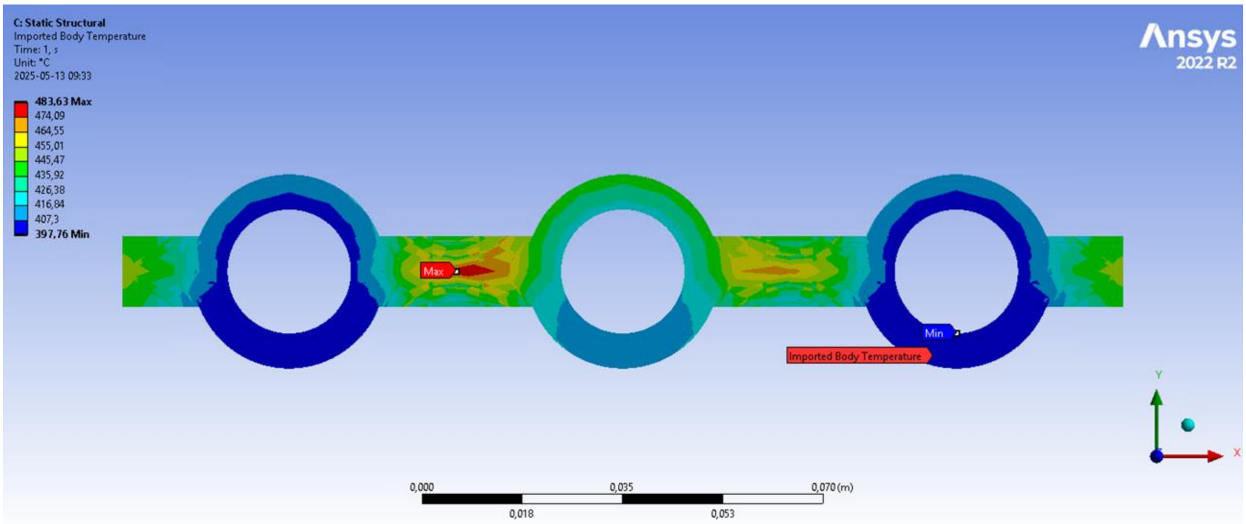

Fig. 12. The temperature distribution in the cross-section of the analysed system with a wider tube spacing at a distance of 120 m from the tube inlet.

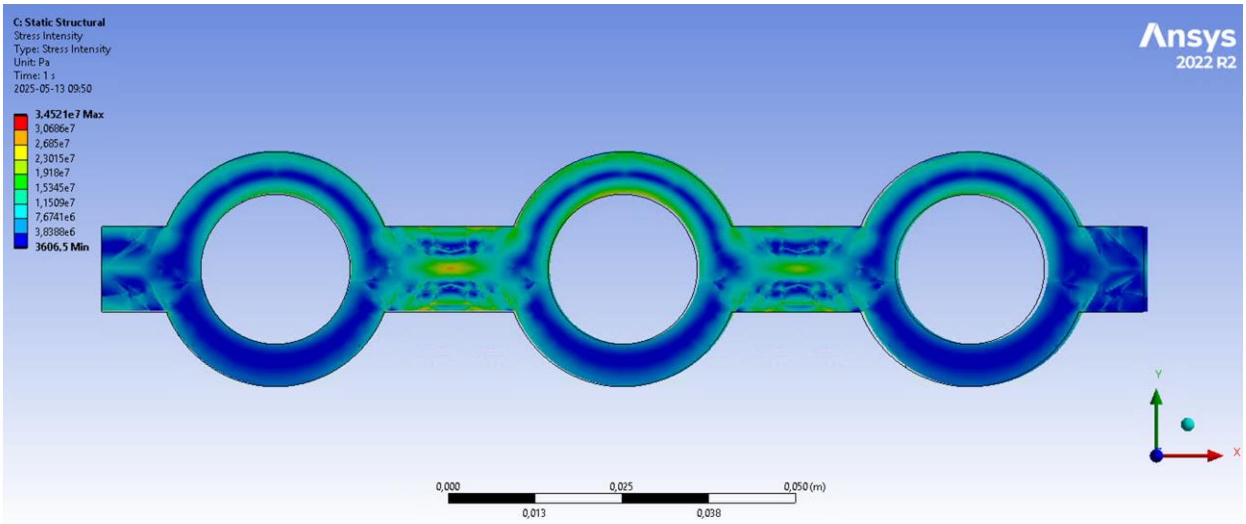

Fig. 13. The thermal stress distribution in the cross-section of the analysed system with "standard" tube spacing at a distance of 40 m from the tube inlet.

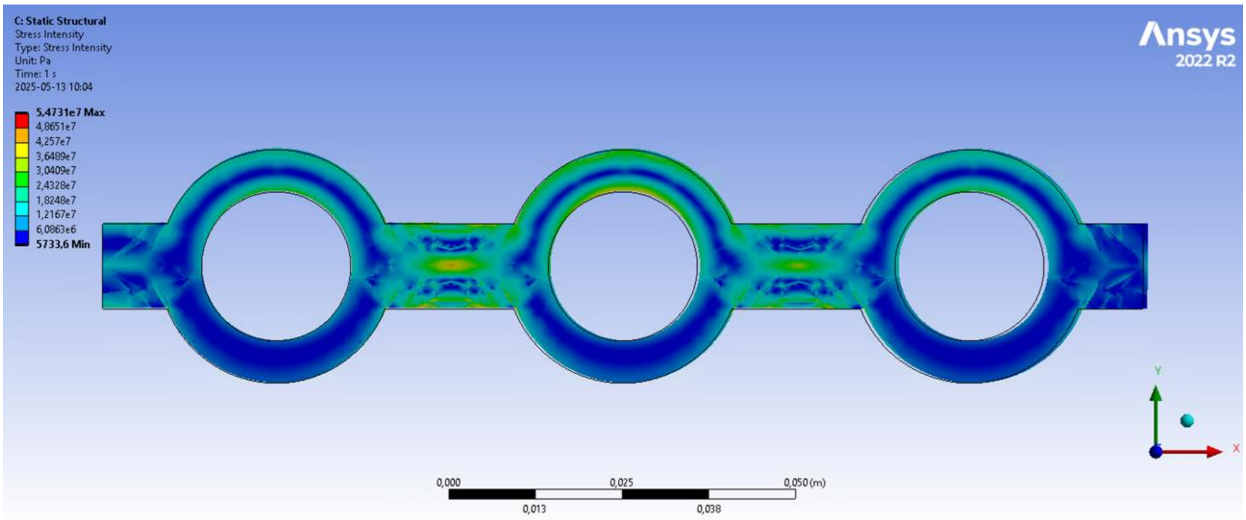

Fig. 14. The thermal stress distribution in the cross-section of the analysed system with "standard" tube spacing at a distance of 80 m from the tube inlet.

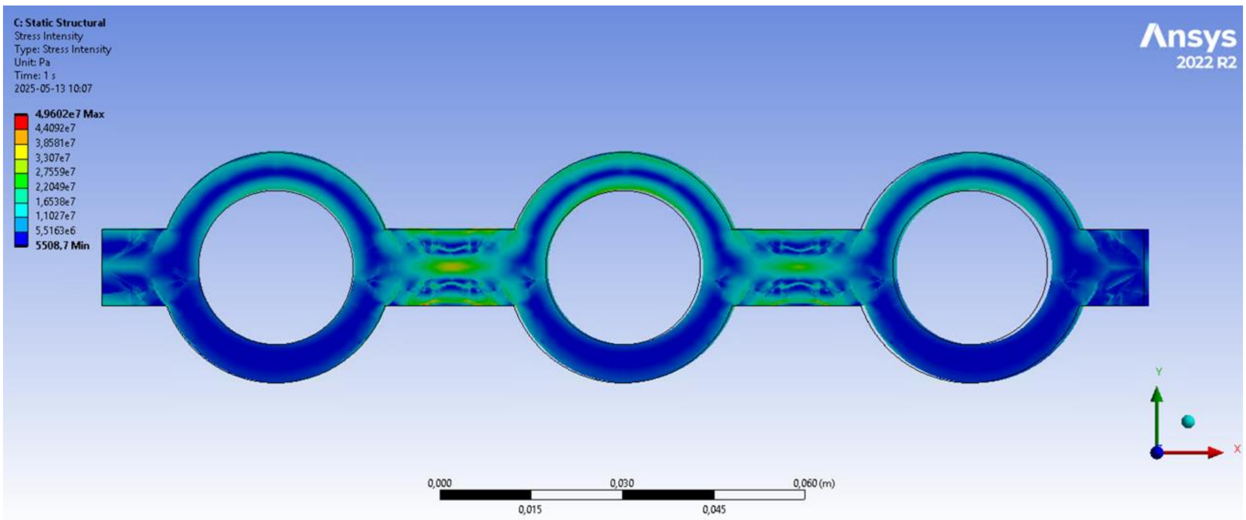

Fig. 15. The thermal stress distribution in the cross-section of the analysed system with "standard" tube spacing at a distance of 120 m from the tube inlet.

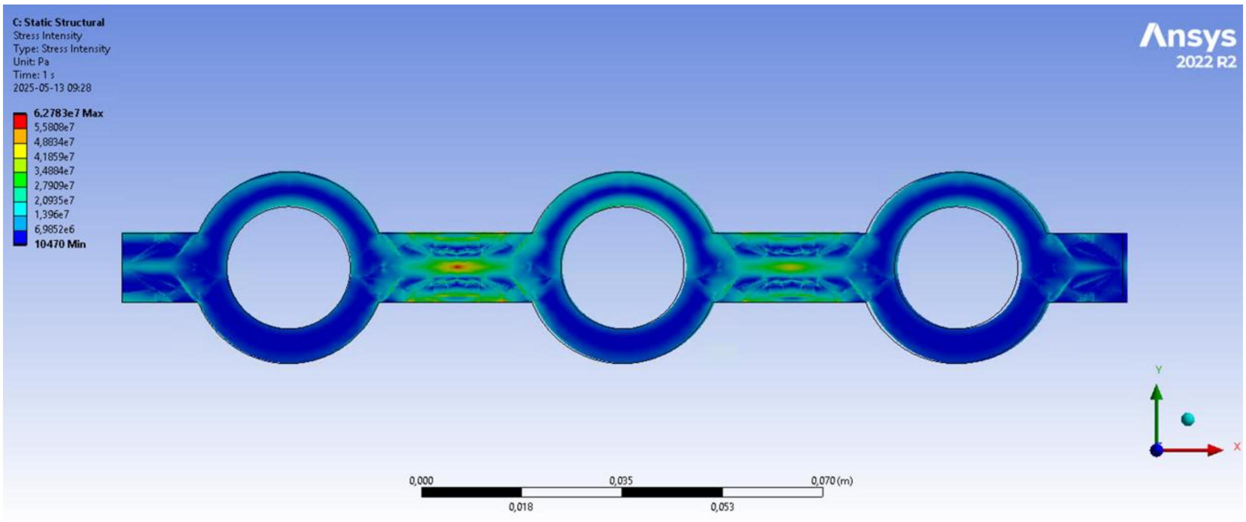

Fig. 16. The thermal stress distribution in the cross-section of the analysed system with wider tube spacing at a distance of 40 m from the tube inlet.

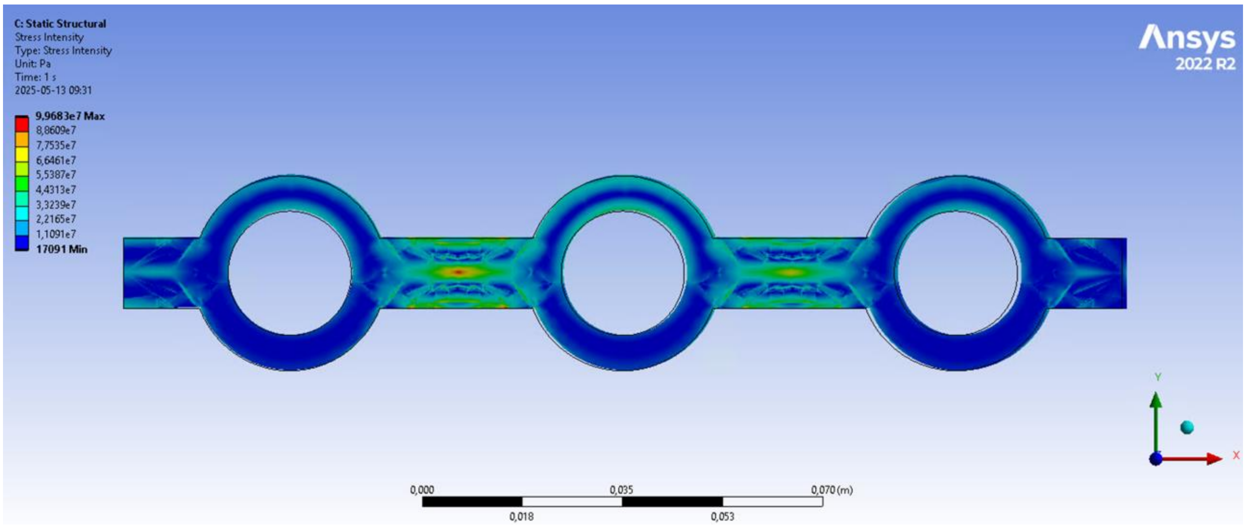

Fig. 17. The thermal stress distribution in the cross-section of the analysed system with wider tube spacing at a distance of 80 m from the tube inlet.

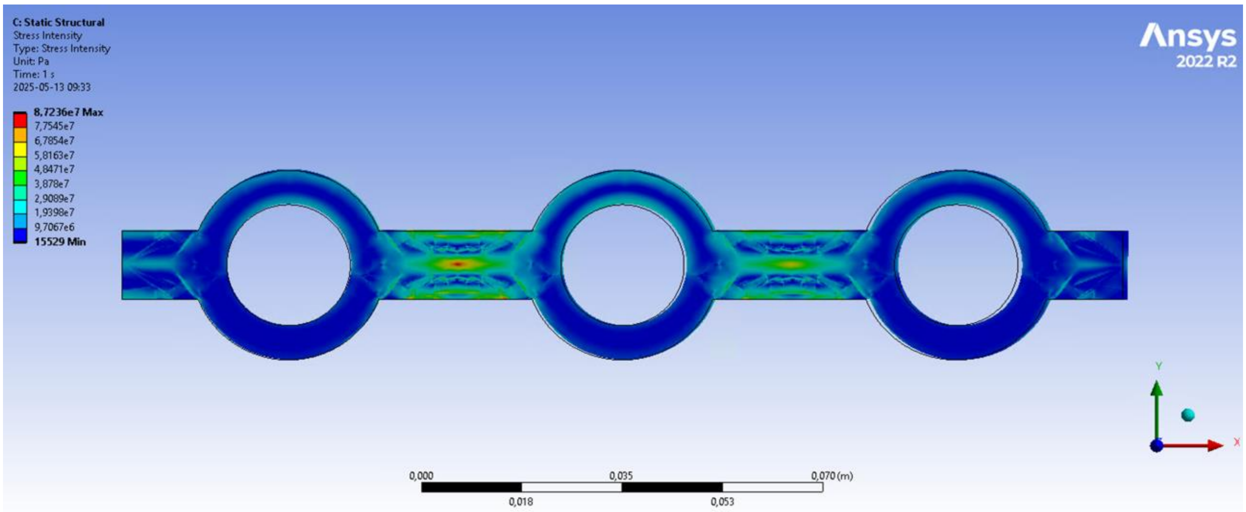

Fig. 18. The thermal stress distribution in the cross-section of the analysed system with wider tube spacing at a distance of 120 m from the tube inlet.

Due to the analysis of a small section of the combustion chamber wall, correctly representing the conditions occurring at the edges of the analysed area was a significant challenge. As it was mentioned before, to approximate the actual simulation conditions, a plane strain state was assumed, meaning that there was no deformation in the *Z*-axis direction perpendicular to the analysed cross-section. One side of the model was fixed to a point, and the other side was blocked from moving relative to the *Y*-axis.

To compare the stresses occurring in the cross-sections of the analysed system depending on the length of the fins connecting the tubes, thermal stress values were determined at the centres of the cross-sections of both fins; they are presented in Table 1. Differences between the stress values for each fin in the same cross-section result from the previously described method of mounting the analysed model.

To facilitate the search for relationships between the obtained stress and temperature values at the analysed points of the system, Table 2 presents the temperature values at points marked with numbers "36" and "71", located at the centres of the fins, for each of the analysed cross-sections of the tubes and fins connecting them.

Table 1. The thermal stress values calculated for the analysed cross-sections of waterwall tubes connected by fins.

Distance from the tube inlet, [m]	Case 1 – „standard" tube spacing		Case 2 – wider tube spacing	
	Thermal stress value in point „36", [MPa]	Thermal stress value in point „71", [MPa]	Thermal stress value in point „36", [MPa]	Thermal stress value in point „71", [MPa]
40	20.69	25.72	44.59	57.34
80	32.07	40.33	70.12	89.23
120	29.19	36.62	62.38	80.16

Table 2. The temperature values calculated for the analysed cross-sections of waterwall tubes connected by fins.

Distance from the tube inlet, [m]	Case 1 – „standard" tube spacing		Case 2 – wider tube spacing	
	Temperature value in point „36", [°C]	Temperature value in point „71", [°C]	Temperature value in point „36", [°C]	Temperature value in point „71", [°C]
40	372.52	367.47	400.97	390.83
80	439.45	431.52	482.90	466.79
120	443.07	436.19	483.81	469.48

6. Conclusions

A new model for determining the distribution of thermal stresses in fragments of combustion chamber walls for the considered cases of tube assembly with different tube spacing was presented. The proposed algorithm allows calculating thermodynamic parameters of the working fluid and wall material for each control volume of the analysed model in each time step. By using this model, it is possible to calculate temperature values in 36 characteristic points of the cross-section of each tube connected with fins. The obtained temperature values are close to the temperature distributions obtained in other scientific papers and by using CFD software.

The novelty of this paper is the comparison of thermal stress values for systems with identical input parameters of the working medium and identical values of the specific heat flux incident on the combustion chamber walls, but with different spacing widths of the waterwall tubes. This allows for an analysis of the effect of the fin width between the tubes on the temperatures and thermal stresses obtained at the centres of fins.

The obtained temperature and thermal stress distributions indicate that as the fin width between the tubes increases, so do the temperatures and thermal stresses. The analysis allows us to conclude that in areas with high heat flux to the combustion chamber walls, it would be beneficial to reduce the spacing of the waterwall tubes to reduce thermal stresses and minimise the risk of damage resulting from exceeding the permissible operating temperatures for the metals from which the tubes and fins are made.

References

[1] Majdak, M., & Grądziel, S. (2016). Thermal flow analysis of vertical combustion chamber waterwall tubes operation. *MATEC Web of Conferences*, 240, 05020. doi: 10.1051/matecconf/201824005020

[2] Taler, J., Węglowski, B., Zima, W., Duda, P., Grądziel, S., Sobota, T., Cebula, A., & Taler, D. (2008). Computer system for monitoring power boiler operation. *Proceedings of the Institution of Mechanical Engineers, Part A: Journal of Power and Energy*, 222(1), 13−24. doi: 10.1243/09576509jpe419

[3] Wang, S., Yang, D., Zhao, Y., & Qu, M. (2018). Heat transfer characteristics of spiral water wall tube in a 1000 MW ultra-supercritical boiler with wide operating load mode. *Applied Thermal Engineering*, 130, 501−514. doi: 10.1016/j.applthermaleng.2017.10.114

[4] Węglarz, K., Taler, D., Taler, J., & Marcinkowski, M. (2023). Numerical modelling of steam superheaters in supercritical boilers. *Energies*, 16, 2615. doi: 10.3390/en16062615

[5] Grądziel, S., & Majewski, K. (2017). Simulation of thermal and flow phenomena in smooth and internally rifled tubes. *Heat Transfer Engineering*, 39(13-14), 1243−1250. doi: 10.1080/01457632.2017.1363633

[6] Grądziel, S., & Majewski, K. (2016). Simulation of temperature distribution and heat transfer coefficient in internally ribbed tubes. *Procedia Engineering*, 157, 44−49. doi: 10.1016/j.proeng.2016.08.336

[7] Majewski, K., & Grądziel, S. (2016). CFD simulations of heat transfer in internally helically ribbed tubes. *Chemical and Process Engineering*, 37(2), 251−260. doi: 10.1515/cpe-2016-0020

[8] Grądziel, S., & Majewski, K. (2019). Experimental determination of the friction factor in a tube with internal helical ribs. *Energies*, 12(2), 257. doi: 10.3390/en12020257

[9] Yamamoto, K., Suganuma, H., Domoto, K., Yamasaki, Y., Kanemaki, Y., & Nakaharai, H. (2013). Design Technology for Supercritical Sliding Pressure Operation Vertical Water Wall Boilers-First Report : History of Practical Application and Introduction of Enhanced Rifled Tube. *Mitsubishi Heavy Industries Technical Review*, 50(3).

[10] Gaćeša, B., Maneski, T.D., Milosevic-Mitic, V.O., Nestorovic, M.S., & Petrovic, A. (2014). Influence of furnace tube shape on thermal strain of fire-tube boilers. *Thermal Science*, 18(1), 39−47. doi: 10.2298/TSCI130317172G

[11] Taler, J., Duda, P., Węglowski, B., Zima, W., Grądziel, S., Sobota, T., & Taler, D. (2009). Identification of local heat flux to membrane water-walls in steam boilers. *Fuel*, 88, 305−311. doi: 10.1016/j.fuel.2008.08.011

[12] Grądziel, S. (2013). Determination of the heat load on the walls of the furnace chamber of the OP-210 boiler. In *Energy machines and devices* (pp. 71−90). Cracow, Poland (in Polish).

[13] Grądziel, S. (2015). Heat load determination of boiler furnace chamber. *Archivum Combustionis*, 35(2), 75−88.

[14] Zima, W., Grądziel, S., & Cebula, A. (2010). Modelling of heat and flow phenomena occurring in water-wall tubes of boilers for supercritical steam parameters. *Archives of Thermodynamics*, 31(3), 19−36. doi: 10.2478/v10173-010-0012-y

[15] Taler, J., Taler, D., & Kowal, A. (2011). Measurements of absorbed heat flux and water-side heat transfer coefficient in water wall tubes. *Archives of Thermodynamics*, 32(3), 77−88. doi: 10.2478/v10173-011-0004-6

[16] Zima, W., Nowak-Ocłoń, M., & Ocłoń, P. (2015). Simulation of fluid heating in combustion chamber water-walls of boilers for supercritical steam parameters. *Energy*, 92, 117−127. doi: 10.1016/j.energy.2015.02.111

[17] Zima, W., & Nowak-Ocłoń, M. (2016). A new 1D/3D model of conjugate heat transfer in waterwall tubes of power boiler combustion chamber. *Procedia Engineering*, 157, 200−206. doi: 10.1016/j.proeng.2016.08.357

[18] Zima, W., Nowak-Ocłoń, M., & Ocłoń, P. (2018). Novel online simulation-ready models of conjugate heat transfer in combustion chamber waterwall tubes of super-critical power boilers. *Energy*, 148, 809−823. doi: 10.1016/j.energy.2018.01.178

[19] Zima, W. (2019). Analysis of temperature drops on the wall thickness of a supercritical boiler water-wall tube. *Thermal Science*, 23(4), 1091−1100. doi: 10.2298/TSCI19S4091Z

[20] Zima, W., Grądziel, S., Cebula, A., Rerak, M., & Kozak-Jagieła, E. (2024). Simulation of the supercritical boiler evaporator operation under conditions of a rapid power increase. *Applied Thermal Engineering*, 243, 122592. doi: 10.1016/j.applthermaleng.2024.122592

[21] Trojan, M., & Taler, J. (2013). Effect of scale deposits on the internal surfaces of the tubes on the superheater operation. *Archives of Thermodynamics*, 34(4), 73−91. doi: 10.2478/aoter-2013-0030

[22] Grądziel, S., & Majewski, K. (2016). Simulation of heat transfer in combustion chamber waterwall tubes of supercritical steam boilers. *Chemical and Process Engineering*, 37(2), 199−213. doi: 10.1515/cpe-2016-0017

[23] Majdak, M., & Grądziel, S. (2020). Influence of thermal and flow conditions on the thermal stresses distribution in the evaporator tubes. *Energy*, 209, 118416. doi: 10.1016/j.energy.2020.118416

[24] Majdak, M., Grądziel, S., Zima, W., Cebula, A., Rerak, M., & Kozak-Jagieła, E. (2024). Numerical and experimental analysis of thermal and flow operating conditions of waterwall tubes connected by fins. *Archives of Thermodynamics*, 44(4), 231−252. doi: 10.24425/ather.2023.149719

[25] Kitoh, K., Koshizuka, S., & Oka, Y. (2001). Refinement of transient criteria and safety analysis for a high temperature reactor cooled by supercritical water. *Nuclear Technology*, 135, 252−264. doi: 10.13182/NT01-A3220